Molecular Neurobiology (2019) 56:13–28
https://doi.org/10.1007/s12035-018-1070-4

Amyloid Precursor Protein Dimerisation Reduces Neurite Outgrowth

Luan Luu[1] · Giuseppe D. Ciccotosto[1,2,3] · Laura J. Vella[3] · Lesley Cheng[4] · Laila C. Roisman[1] · Gerhard Multhaup[5] · Andrew F. Hill[4] · Lisa-Marie Munter[5] · Roberto Cappai[1,2]

Received: 14 December 2017 / Accepted: 9 April 2018 / Published online: 19 April 2018

Abstract

The amyloid precursor protein (APP) undergoes extensive metabolism, and its transport and proteolytic processing can be modulated by its ability to form a homodimer. We have investigated the functional consequences of stabilised APP dimer expression in cells by studying the engineered dimerisation of the APP_{L17C} (residue 17 in Aβ sequence) construct, which is associated with a 30% increase in APP dimer expression, on APP's neurite outgrowth promoting activity. Overexpression of APP_{L17C} in SH-SY5Y cells decreased neurite outgrowth upon retinoic acid differentiation as compared to overexpressing APP_{WT} cells. The APP_{L17C} phenotype was rescued by replacing the APP_{L17C} media with conditioned media from APP_{WT} cells, indicating that the APP_{L17C} mutant is impairing the secretion of a neuritogenic promoting factor. APP_{L17C} had altered transport and was localised in the endoplasmic reticulum. Defining the molecular basis of the APP_{L17C} phenotype showed that RhoA GTPase activity, a negative regulator of neurite outgrowth, was increased in APP_{L17C} cells. RhoA activity was decreased after APP_{WT} conditioned media rescue. Moreover, treatment with the RhoA inhibitor, Y27632, restored a wild-type morphology to the APP_{L17C} cells. Small RNAseq analysis of APP_{L17C} and APP_{WT} cells identified several differentially expressed miRNAs relating to neurite outgrowth. Of these, miR-34a showed the greatest decrease in expression. Lentiviral-mediated overexpression of miR-34a rescued neurite outgrowth in APP_{L17C} cells to APP_{WT} levels and changed RhoA activation. This study has identified a novel link between APP dimerisation and its neuritogenic activity which is mediated by miR-34a expression.

Keywords Amyloid precursor protein · Neurite · microRNA · Function · Dimerisation · RhoA

Introduction

The amyloid precursor protein (APP) is an integral type I transmembrane glycoprotein that is enriched in the central nervous system. APP is processed through distinct proteolytic pathways into various secreted and intracellular fragments, and these APP metabolites affect a range of cellular functions [1] including neuritogenesis, metal homeostasis, neuronal development, cell-cell interactions, cell signalling, blood coagulation, glucose homeostasis and neuroprotection [2, 3]. The regulation of APP metabolism can occur through mutations that affect APP transport and/or cleavage by the secretases [4] as well as its interaction with cofactors such as metals [5] and proteoglycans [6] and function as a receptor protein [7]. APP can also undergo oligomerisation and form homodimers either via ectodomain interactions [8] and the three GxxxG transmembrane dimerisation motifs (G25, G29 and G33) [9] located in the Aβ peptide sequence (Fig. 1a). Substitution of the glycine residues with either isoleucine or alanine reduces transmembrane dimerisation strength and decreases the production of Aβ42 [9, 10]. However, promoting dimerisation by substituting a cysteine residue for a leucine near the juxtamembrane region (residue 17 in Aβ sequence (L17C) or residue 613 in APP695 sequence) creates disulphide-linked dimers, which causes decreased cleavage and secretion of sAPPα and decreased production of Aβ40 and Aβ42 and concomitant increased production of Aβ38 peptide [9].

✉ Roberto Cappai
r.cappai@unimelb.edu.au

1 Department of Pathology, The University of Melbourne, Melbourne, VIC 3010, Australia

2 Department of Pharmacology & Therapeutics, The University of Melbourne, Melbourne, VIC 3010, Australia

3 Florey Institute of Neuroscience and Mental Health, The University of Melbourne, Melbourne, VIC 3010, Australia

4 Department of Biochemistry and Genetics, La Trobe Institute for Molecular Science, La Trobe University, Bundoora, VIC 3086, Australia

5 Department of Pharmacology & Therapeutics, McGill University, Montreal, QC H3G 1Y6, Canada

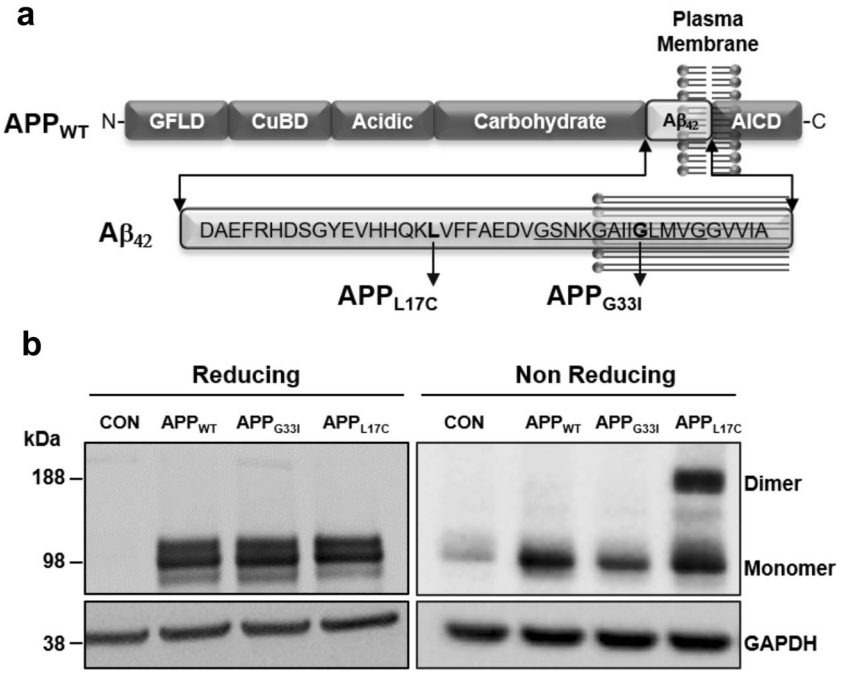

Fig. 1 Stably transfected SH-SY5Y cell line expressing APP_{L17C} expresses APP homo dimers. **a** Illustration of the full-length wild-type APP (APP_{WT}) showing the major domain structures (growth factor like domain (GFLD), copper binding domain (CuBD), acidic, carbohydrate, APP intracellular domain (AICD)) and the Aβ42 peptide sequence highlighting the dimerisation GxxxG motif (underlined amino acids) and sites of the point mutations for APP_{L17C} and APP_{G33I}. **b** Stably transfected vector only control (CON), APP_{WT}, APP_{G33I} and APP_{L17C} SH-SY5Y cell lines were differentiated for 14 days in media supplemented with 10 μM retinoic acid and western blot analysis of cell lysates showing monomeric and homodimer APP structures were detected using mAb 22C11. Lysate samples were prepared in sample buffer containing BME (reducing) showing only a monomeric APP band, while cell lysates prepared in minus BME (Non Reducing) conditions showed a monomeric APP in all cell lysates and a dimer band only in the APP_{L17C} sample. Western blots are representative of four individual experiments and GAPDH detected and used as a loading control

The relationship between APP dimerisation and APP function, beyond its effects on APP proteolytic processing and transport, is not understood. In this study, we examined the effect of the L17C mutation has the neuritogenic activity of APP. APP's regulation of neurite outgrowth has been confirmed both in in vivo and in vitro studies where endogenous expression or exogenous presence of APP promotes neurite outgrowth, axonal sprouting and dendritic growth [11–14]. A transient decrease in cellular APP expression resulted in reduced neurite growth in both axons and dendrites [15]. Our study has found that stable expression of APP_{L17C} in SH-SY5Y cells, which promotes the cellular expression of APP homodimer formation, causes the downregulation of neurite outgrowth. The molecular basis for this effect was attributed to an alteration in secreted neuritogenic factor(s), upregulation in RhoA activity (a neuritogenesis inhibitor) and a marked decrease in expression of the microRNA miR-34a which is associated with regulation of neurite outgrowth.

Method

Reagents and Antibodies

Antibodies used were anti-APP 22C11 (APP 66-81) produced in-house, β3-tubulin (D71G90) and glyceraldehyde 3-phosphate dehydrogenase (GAPDH, #2188) from Cell Signalling Technologies (Danvers, MA, USA), GRASP64 (Ab30315) and calnexin (Ab22595) were sourced from Abcam (VIC, Australia). All chemicals were obtained from Sigma-Aldrich (NSW, Australia), and all cell culture media were obtained from Thermo Fisher Scientific (VIC, Australia) unless otherwise indicated. Recombinant sAPP695 was expressed and purified from human HEK293T cells as previously described [16]. Purity was confirmed by mass spectrometry and sodium dodecyl sulfate-polyacrylamide gel electrophoresis.

Neuronal Cell Line

SH-SY5Y human neuroblastoma cells (American Type Culture Collection, Rockville, MD, USA) were grown in DMEM supplemented with 10% heat-inactivated fetal calf serum, 1 U/mL of penicillin, 1 μg/mL of streptomycin and 2 mM glutamate and maintained at 37 °C and 5% CO_2. Cells were differentiated so that they would display a neuronal phenotype, including extensive neurites and branching. To obtain differentiated cells, 2×10^5 cells were plated in 1 well of a 6-well plate and allowed to adhere for 24 h. Differentiation was started in DMEM supplemented with 1.5% fetal calf serum and 10 μM retinoic acid. Cell culture media was replaced with fresh DMEM containing retinoic acid and 1.5% fetal calf serum every 3 days.

Experiments were performed on cells differentiated for 0, 7 or 14 days.

Plasmids, Transfections and pLenti Virus Transduction

The generation of the full-length APP695 wild-type (APP) and mutant (APP_{L17C} and APP_{G33I}) constructs were prepared using previously described procedures [9]. Briefly, cDNAs encoding for APP were inserted into a pCEP4 vector, which contains a hygromycin B resistance gene for stable selection in transfected cells; then, respective APP codons were mutated by site-directed mutagenesis. For lentiviral expression, cDNAs were transferred from pCEP4 into a lentiviral vector (Invitrogen, VIC, Australia). The control empty vector GFP (GFP-CON) and GFP-miR-34a lentiviral constructs were sourced as premade lentiviruses from Gentarget (San Diego, CA USA) and used according to the manufacturer's instructions. These lentivector constructs contain a GFP protein sequence that indicates miRNA expression and a puromycin resistance gene that allows for antibiotic selection and stable expression.

SH-SY5Y cells were seeded onto 24-well plates at a density of 62,500 cells/cm^2 and left overnight in a 37 °C incubator supplemented with 5% CO_2. On the following day, the growth media was replaced with serum free Opti-MEM, and for stable transfection of APP_{WT}, APP_{L17C} or APP_{G33I}, constructs and plasmids (5 μg) were transfected using LipofectAMINE 2000 (Invitrogen, VIC, Australia) following the manufacturer's instruction. Stably transfected cells were selected with hygromycin-B (100 μg/mL), and cells were analysed for transgene expression by Western blot and histochemical analysis. Premade lentivirus-miRNA particles were obtained from GenTarget and transduced into cells according to the manufacturer's instructions (GenTarget, San Diego, CA, USA). The APP_{L17C} expressing SH-SY5Y cells were seeded onto 12-mm-diameter glass coverslips placed in 24-well plates containing complete DMEM media and were transfected with either the GFP-CON or GFP-miR-34a vector. Cells were transfected under two different conditions: (a) prior to differentiation where cells were transfected 24 h after seeding and differentiated for 14 days or (b) post-differentiation where cells were allowed to differentiate for 14 days and were then transfected.

Western Blotting

For Western blot analysis, cells were lysed in ice-cold lysis buffer (25 mM HEPES, 100 mM NaCl, 1 mM EDTA, 10% (*v*/*v*) glycerol, 1% (*v*/*v*) Triton X-100) containing protease inhibitor mix (Roche) and protein concentration was determined by BCA assay (Gibco BRL, ThermoFisher). Conditioned media was collected 3 days after media change and centrifuged at 10,000×*g* for 3 min, and total secreted protein was extracted with 25% trichloroacetic acid. For reducing conditions, samples were then diluted in 2× sample buffer (125 mM Tris-HCl, pH 6.8, 5% BME, 4% SDS, 10% glycerol and 0.02% bromophenol blue, *w*/*v*), boiled for 3 min at 95 °C, then centrifuged for 2 min at 12,000×*g*, before being electrophoresed on precast 12% Bis-Tris NuPage gels (Invitrogen). Gels were electrophoresed at 150 V in MES buffer (50 mM Tris Base, 1 mM EDTA and 3.4 mM SDS) for 1 h. Proteins were transferred onto nitrocellulose membrane (Bio-Rad) and then blocked in 5% skim milk powder in PBST (PBS with 0.5% Tween-20) for 1 h. Membranes were probed with primary antibody diluted in PBS-T containing 5% skim milk powder overnight, washed with PBS-T and then probed with horseradish peroxidase-conjugated secondary antibody for 1 h. Immunoreactivity was detected by enhanced chemiluminescence (GE Healthcare) and imaged on Microchemi (DNR Bio-Imaging Systems). Densitometric analysis of band intensities was performed from images and quantified using ImageJ software (NIH ver1.48). Blots were probed with antibodies 22C11 (1:500), β3-tubulin (1:5000) and GAPDH (1:5000).

Phase Contrast and Immunofluorescence Histochemical Analysis

For phase contrast images, SH-SY5Y cells were grown in 6-well plates and images were taken using Leica DM IRB inverted microscope using a 20× objective and a Zeiss axiocam MRc camera, and Axiovision software (Zeiss, Australia) was used to acquire the images. For immunofluorescence microscopy, cells were initially fixed in 4% formaldehyde followed by permeabilisation (0.075% Triton X-100), blocking (10% goat serum) and incubation with primary antibodies. Cells were then washed in PBS buffer several times before incubating with either an anti-rabbit Alexa 567 (1:500) and/or anti-mouse Alexa 488 (1:500) secondary antibody plus 4′,6-diamidino-2-phenylindole (DAPI) then washed in several rinses of PBS before they were finally mounted onto glass slides using Prolong Gold mounting medium (Invitrogen, VIC, Australia). The cell immunofluorescence was imaged using a Zeiss Axioscope 2 microscope with a 40× objective lens. Images were taken using a Photometrics Coolsnap ES2 monochrome camera and Zen 2.0 software (Zeiss, Australia). Images are representative of three independent experiments. Primary antibodies 22C11 (1:50), β3-tubulin (1:100), calnexin (1:100) and GRASP64 (1:100) were used. Neurite counts (40–80 cells from in four independent experiments) and neurite lengths (~90 neurites from four independent experiments) were quantitated from phase contrast or immunofluorescent images using ImageJ software (NIH).

MicroRNA Isolation, Library Preparation and Deep Sequencing

Total RNA was isolated from SH-SY5Y cells using the miRNeasy kit (Qiagen, VIC, Australia) according to the

manufacturer's instructions. RNA integrity and concentration were assessed using the RNA Nano 6000 chip and run on the Agilent 2100 Bioanalyser (Agilent Technologies, VIC, Australia). Small RNA was further isolated from total RNA using the NEBNext Poly(A) mRNA magnetic isolation module (New England BioLabs, Ipswich, MA USA) according to the manufacturer's instructions. The yield and size distribution of mRNA was analysed on the Agilent 2100 Bioanalyser using an RNA Nano 6000 chip.

The enriched RNA was prepared for cDNA synthesis and library construction using Ion Total RNA-Seq Kit v2 for Small RNA Libraries following the manufacturer's instructions (Life Technology, publication part #4476289). Samples were ligated to unique indexed barcoded primers during PCR amplification to generate a barcoded library for sequencing. The cDNA was then purified using nucleic acid binding beads according to the manufacturer's protocol (Ion Total RNA-Seq Kit v2 for Small RNA Libraries, from Life Technologies, VIC, Australia). cDNA concentration and size was determined using the Agilent Bioanalyser and Agilent DNA 1000 Kit (Agilent Technologies, VIC, Australia).

Ion PMG Template OT2 200 Kit (ThermoFisher, VIC, Australia) was used to amplify and load the enriched cDNA library onto Ion Sphere Particles. Since not all Ion Sphere Particles are loaded with cDNA, only template-positive Ion Sphere Particles were recovered using the Dynabeads MyOne™ Streptavidin C1 Beads and the Ion OneTouch™ ES instrument. The final sequencing step used the Ion PMG sequencing 200K v2 to prepare the template-positive Ion Sphere Particles to be loaded onto the Ion 318™ Chip v2 BC and sequenced on the Ion PGM™ Sequencer. Sequence results were aligned to the human genome and mapped to miRBase v.19. The data was analysed for differential expression and fold changes using Partek Genomic Suite software (Partek, Singapore). Reads were normalised to reads per million calculated as by number of sequenced reads/total reads × 1,000,000.

RhoA GLISA Activation Assay

The activity of RhoA was established using the RhoA G-LISA Activation Assay Kit BK124 (Cytoskeleton, Denver, CO, USA) following the manufacturer's instructions. Briefly, differentiated SH-SY5Y cells were washed with ice-cold PBS, lysed on ice and protein concentration of the lysate measured using the Precision Red Advanced Protein Assay reagent (Cytoskeleton, Denver, CO, USA) and adjusted to 0.5 mg/mL. GLISA wells were incubated with the cell lysates on an orbital shaker at 4 °C for 30 min. Wells were washed, incubated with anti-RhoA primary antibody for 30 min at RT, washed and incubated with horseradish peroxidase-labelled secondary antibody for 45 min at RT. The detection reagent was added to each well and incubated 37 °C for 15 min, and the reaction stopped with HRP stop buffer. Plates were read at 490 nm on a spectrophotometer. Blanks were subtracted from individual wells and activity of RhoA calculated relative to vector control or untreated wells.

qRT-PCR Validation

SH-SY5Y cells were lysed in QIAzol Lysis buffer and RNA extracted using a miRNeasy Mini Kit according to the manufacturer's protocol (Qiagen, VIC, Australia). RNA quality and quantity were then assessed using Agilent RNA 6000 Nano chip and Agilent Bioanalyser according to the manufacturer's protocol (Agilent, VIC, Australia). RNA (400 ng) was converted to cDNA using the TaqMan cDNA Reverse Transcription Kit (Applied Biosystems, Foster City, CA, USA) according to the manufacturers' protocol. qRT-PCR using TaqMan Fast Advanced Master Mix (Applied Biosystems, Foster City, CA, USA) was performed on 1:10 diluted cDNA product using individual gene assays (TaqMan gene assays, 20×, Applied Biosystems, Foster City, CA, USA) and run on the VIIA™ 7 Real-Time PCR System (Life Technologies, VIC, Australia). Each APP mutant was run in triplicate to monitor technical variability and quality control. Data was normalised across the samples using U6 as an endogenous control gene. $2^{-\Delta\Delta Ct}$ method was used to normalise the Ct values of each gene, and determination of fold differences in miRNA expression (normalised to vector control) was calculated. DataAssist (Applied Biosystems, Foster City, CA, USA) was used to analyse the data.

pLenti-miRNA

The pLenti-miR constructs were purchased from GenTarget Inc., San Diego, CA, that corresponded to miR34a (hsa-miR-34a-3p (MIMAT0004557) and hsa-miR-34a-5p (MIMAT0000255)).

Statistical Analysis

Results are expressed as mean ± SEM. Statistical differences were determined using Student's *t* tests or ANOVA with multiple comparison tests with two-tailed analysis with Dunnett or Welch's corrections. Statistical significance was set to a minimum of $p < 0.05$. Graphing and statistical tests were done using GraphPad Prism 6.

Results

The SH-SY5Y APP_{L17C} Cell Line Displays Modified APP Subcellular Localisation to ER and Not Golgi Markers

We previously showed that an amino acid motif $G_{29}xxxG_{33}$, which is located within the Aβ peptide region of the APP695 (APP_{WT}) transmembrane sequence (TMS), can regulate the

extent of APP non-covalent homodimerisation [9]. To examine the effect the stabilised APP dimerisation had on APP's neuritogenic activity, we utilised the APP_{L17C} mutant construct which we previously showed will form approximately 30% of covalent S-S bridged APP dimers. In contrast, the APP_{G33I} mutant decreased APP homodimer expression which abolished Aβ40 and Aβ42 production and replaced it with increased Aβ38 levels in stably transfected SH-SY5Y cells [9]. As expected, the stably transfected SH-SY5Y cells expressing APP_{WT}, APP_{G33I} or APP_{L17C} constructs expressed similar levels of the cellular APP which migrated as a monomer at approximately 100 kDa under reducing conditions (Fig. 1b, reducing). When the cell lysates were prepared in non-reducing conditions (BME minus loading sample buffer), only the SH-SY5Y APP_{L17C} cells, which can form a covalent S-S bridge between adjacent APP proteins, contained a homodimer band that migrated at approximately 190 kDa on the Western blot (Fig. 1b, non-reducing).

To examine whether stabilising the expression of APP dimerisation affected APP's subcellular distribution in differentiated SH-SY5Y cells, we colocalised APP with ER and Golgi markers by fluorescence microscopy (Fig. 2). In CON

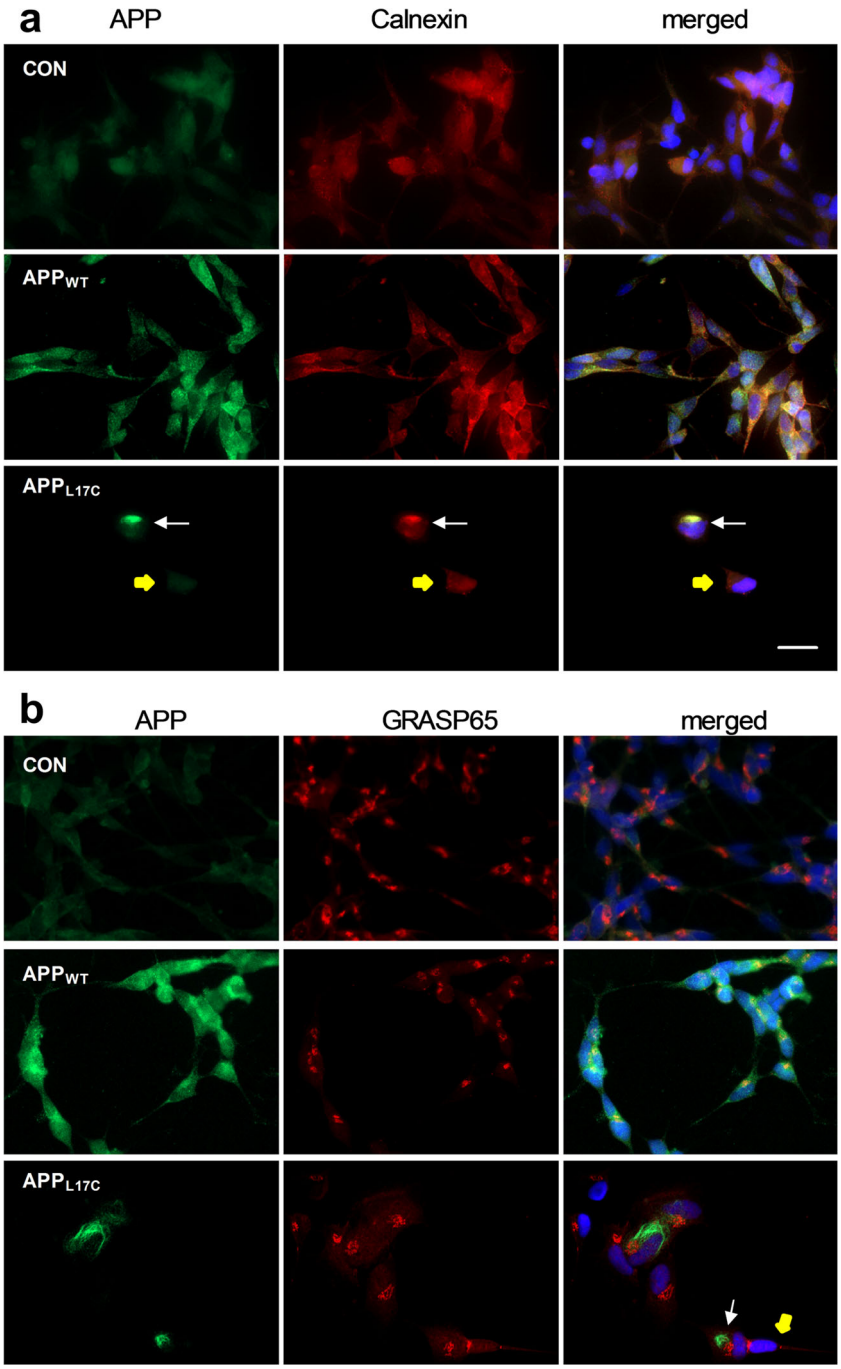

Fig. 2 The SH-SY5Y APP_{L17C} cell line displays a modified APP expression pattern showing intense punctate perinuclear localisation and found to colocalise with ER and not golgi organelle marker. **a**, **b** Stably transfected vector control (CON), APP_{WT} and APP_{L17C} SH-SY5Y cell lines were differentiated for 14 days in 10 μM retinoic acid and immunostained for APP using mAb 22C11 (green) and costained with organelle markers (red) for ER (**a**), by staining for calnexin, for golgi by staining with GRASP65 (**b**), and nucleus using DAPI (blue). A cell showing perinucleur overexpression of APP_{L17C} (white arrow) and a cell lacking APP expression (yellow arrow). Images are representative of three different experiments. Scale bar = 20 μm

(empty vector) and APP_{WT} cells, APP was mainly expressed in very small vesicular compartments throughout the cell cytosol, and we observed strong colocalisation of APP green fluorescence with calnexin, an ER marker as shown by the presence of yellow colour in the merged image (Fig. 2a). However, in the SH-SY5Y cells expressing the mutant APP_{L17C}, APP immunoreactivity was predominantly localised to a perinuclear region in the cell. Surprisingly, the APP immunoreactivity in the APP_{L17C} cells did not colocalise with the Golgi marker GRASP65; rather, it strongly colocalised with the ER marker calnexin (Fig. 2b). The presence of the APP dimer has affected the distribution of the ER organelle such that the ER compartment is compacted and localised to the perinuclear region (Fig. 2a, white arrow), while in the cell that failed to take up APP_{L17C}, the ER can clearly be seen dispersed evenly throughout the cell cytosol (Fig. 2a, yellow arrow). Therefore, the distribution of APP in these APP_{L17C} cells is severely comprised and leads to changes in subcellular localisation.

APP Dimerisation in APP_{L17C} Cells Reduces Neurite Outgrowth and Is Associated with Reduced β3-Tubulin Immunoreactivity

To examine if dimerisation affected APP's neuritogenic activity, the different SH-SY5Y cell lines were treated with retinoic acid (RA) for 2 weeks to induce cellular differentiation. Neurite outgrowth and branching was seen for the CON, APP_{WT} and APP_{G33I} expressing cell lines. However, the APP_{L17C} expressing cell body was elongated and had less neurite branching (Fig. 3a). The number of neurites per cell body were counted, and we observed a similar number of neurites per cell body for the CON, APP_{WT} and APP_{G33I} cell lines, while for the APP_{L17C} cells, the number of neurites per cell body was decreased by 5-fold and was significantly different to the other three lines (Fig. 3b).

The decrease in neurite number was also assessed biochemically by measuring the protein expression level of β3-tubulin, the main cytoskeletal component of neurites [17]. In the CON and APP_{WT} cells, the β3-tubulin expression was readily detectable in the cell soma and neurites. In contrast, the β3-tubulin expression level in the mutant APP_{L17C} cells was markedly decreased—this is illustrated in Fig. 4a showing that two adjacent cells with one cell that lacked APP immunoreactivity showed high levels of β3-tubulin immunoreactivity (Fig. 4a, APP_{L17C} merged image, yellow arrow), while the other cell displayed high expression levels of APP immunoreactivity in the perinuclear region and lacked β3-tubulin expression (Fig. 4a, APP_{L17C} merged image, white arrow). The β3-tubulin expression level in APP_{L17C} cells was examined by Western blot analysis, and the densitometric analysis showed a 2-fold decrease in expression level and significantly different compared to the CON cells (Fig. 4b).

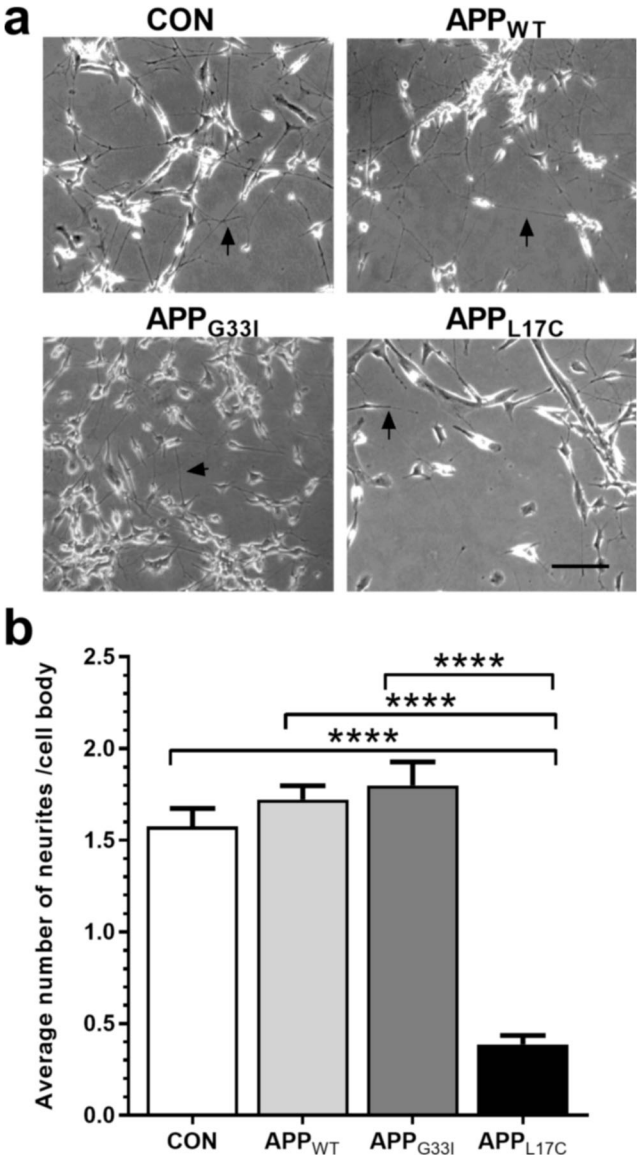

Fig. 3 APP dimerisation reduces neurite outgrowth. **a** Histological phase contrast images of stably transfected vector control (CON), APP_{WT}, APP_{G33I} and APP_{L17C} SH-SY5Y cells differentiated for 14 days in media supplemented with 10 μM retinoic acid. **b** The average number of neurites per cell body (arrows pointing to neurites) was quantitated from 80 cells in four independent experiments. Values are mean ± SEM. $N = 4$, $^{****}p < 0.0001$. Scale bar 100 μm

The APP_{L17C} Defective Neurite Outgrowth Phenotype Was Rescued by Treatment with CON or APP_{WT} Conditioned Media

To examine whether a secretory factor was involved in the APP_{L17C} defective neurite outgrowth phenotype, conditioned media from the different cell lines were collected, TCA precipitated and the presence of soluble APP detected by western blot analysis (Fig. 5a). Densitometric analysis showed that there was a significant decrease in soluble APP present in the media from APP_{L17C} cells compared to the CON cells,

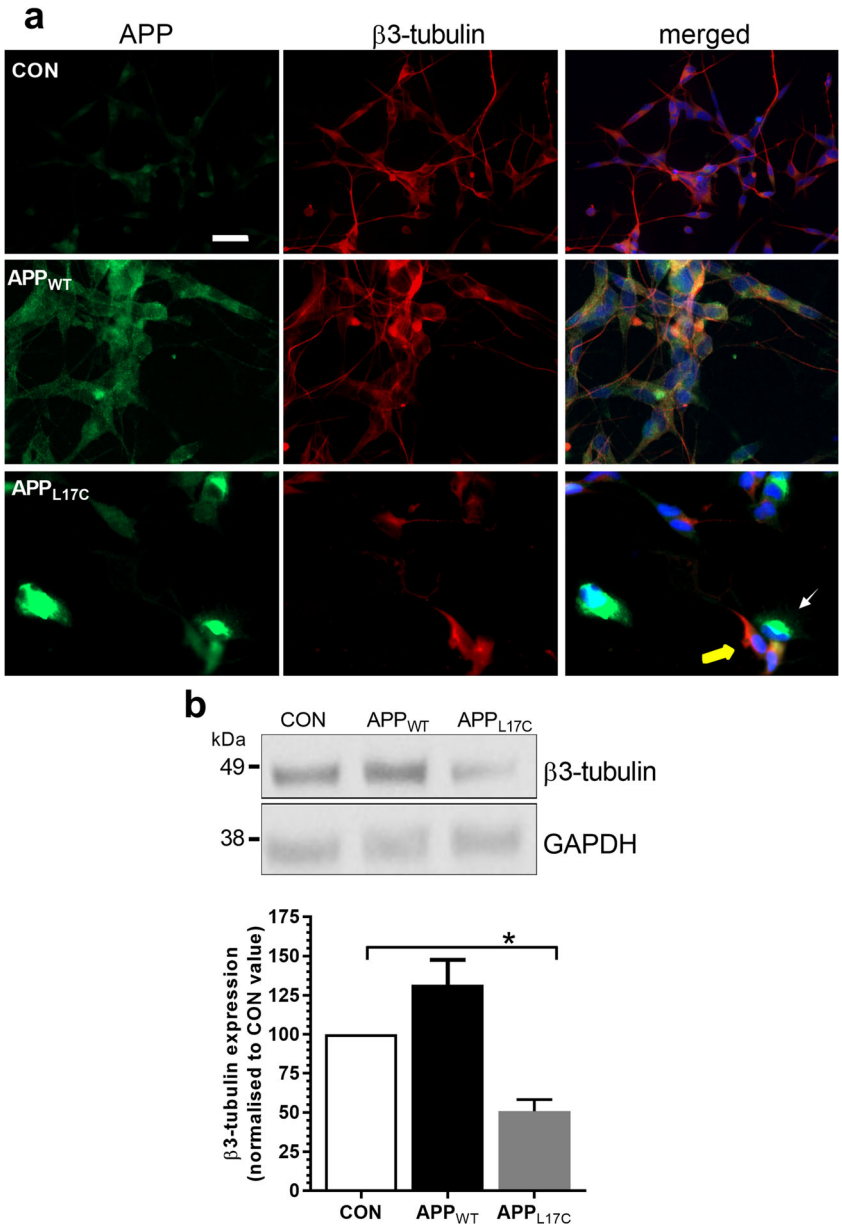

Fig. 4 APP dimerisation in APP_{L17C} cells is associated with reduced β3-tubulin immunoreactivity. **a** Stably transfected vector control (CON), APP_{WT} and APP_{L17C} SH-SY5Y cell lines differentiated for 14 days in media supplemented with 10 μM retinoic acid were immunostained for APP using mAb 22C11 (green), β3-tubulin (red), and merged images showing DAPI (blue) stained nucleus. A cell showing perinucleur overexpression of APP_{L17C} (white arrow) and a cell lacking APP expression (yellow arrow). Images representative of three different experiments. **b** Expression of β3-tubulin was examined by western blot analysis, and subsequent densitometric analysis of the protein band intensities (normalised relative to CON values) was determined. GAPDH levels were detected and used as a loading control. Values are mean ± SEM. $N = 4$, $^*p < 0.05$. Scale bar = 20 μm

while both APP_{WT} and APP_{G33I} cells contained increased APP levels in the media, but it was not statistically different to the CON cells (Fig. 5b). Since APP secretion was compromised in the APP_{L17C} cells, we examined whether the conditioned media from CON or APP_{WT} cells could rescue the APP_{L17C} neurite outgrowth phenotype. The APP_{L17C} cell culture conditioned media was replaced with conditioned media from 14-day-old differentiated CON and APP_{WT} cells, and their morphological appearance was examined 3 days later (Fig. 5c). The addition of conditioned media from CON and APP_{WT} cells caused a significant increase in the number of neurites per cell body (Fig. 5d) to APP_{WT} levels as observed in CON-differentiated cell (Fig. 3b). β3-Tubulin levels in the APP_{L17C} cells were examined by Western blot analysis, and densitometric quantitation showed that β3-tubulin/GAPDH expression was approximately 50% higher following treatment with conditioned media from CON or APP_{WT} cultures compared to the APP_{L17C} cells maintained in its own culture media but did not reach statistical significance (Fig. 5e). Since sAPP is reduced in the APP_{L17C} culture media, we tested if sAPP itself can rescue APP_{L17C} defective neurite outgrowth. APP_{L17C}, CON and APP_{WT} cells were differentiated for 14 days, and then, 0, 10 or 100 nM sAPP695 was added to the culture media. After 3 days in culture, the number of neurites per cell body was quantitated. The sAPP695 caused a significant increase in neurites per cell body in the APP_{L17C} cells with either 10 or 100 nM doses (Fig. 5f). It had no effect on the CON and APP_{WT} cells, suggesting that sAPP levels in those lines were saturated.

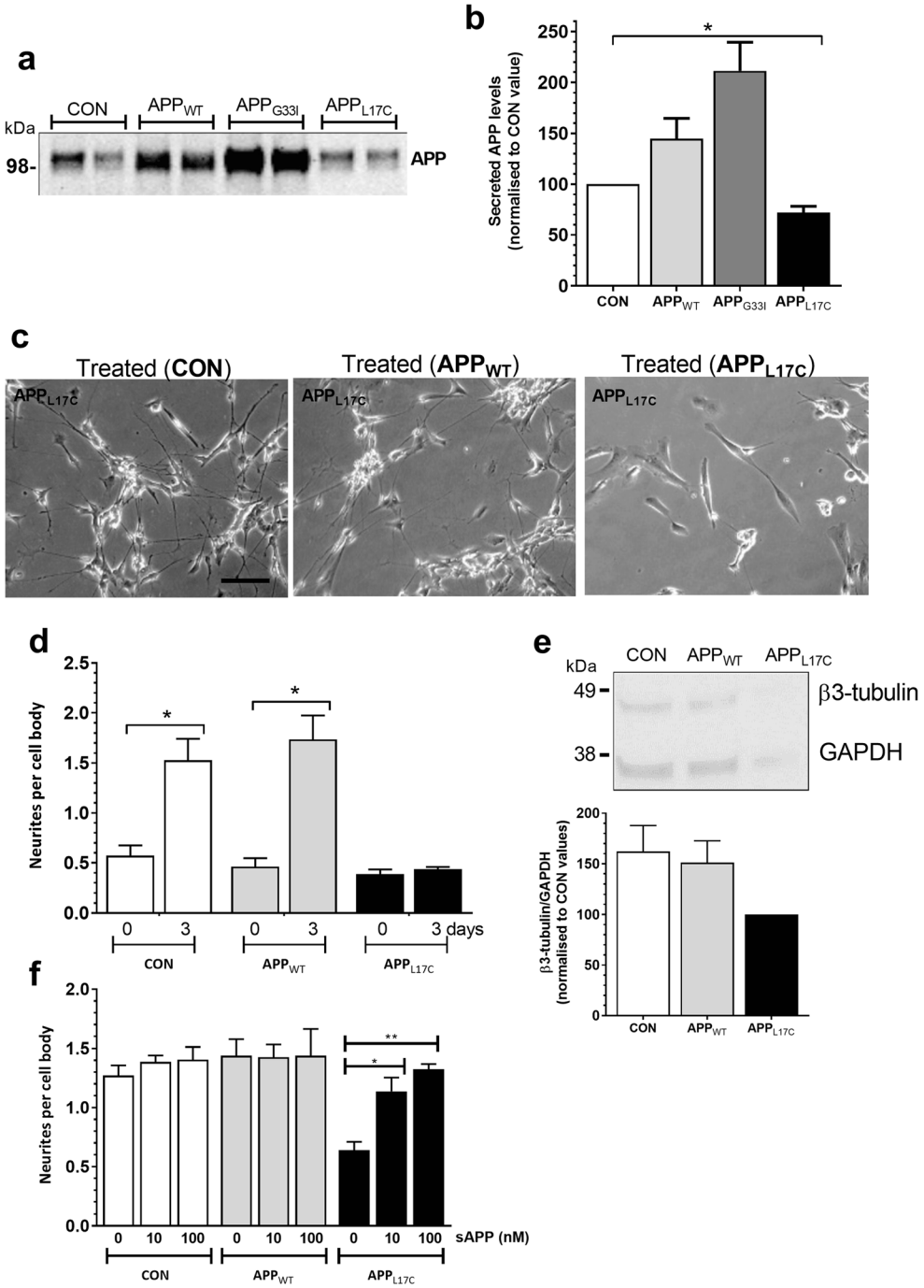

Fig. 5 The APP_{L17C} mutant cell line has diminished APP levels in conditioned media, and its defective neurite outgrowth morphology was rescued by treatment with the conditioned media taken from CON or APP_{WT} cell cultures. **a**, **b** Representative western blot analysis of conditioned media was collected from stably transfected vector control (CON), APP_{WT}, APP_{G33I} and APP_{L17C} SH-SY5Y cells that had been differentiated for 14 days probed for APP immunoreactivity (**a**), and densitometric analysis of APP protein band intensities (normalised relative to CON values) was determined from three independent experiments (**b**). **c**–**e** The APP_{L17C} transfected SH-SY5Y cell line treated for 0 and 3 days using conditioned media taken from the CON, APP_{WT} and APP_{L17C} SH-SY5Y cells differentiated for 14 days and the morphological changes was assessed by taking phase contrast images (**c**) and quantitating the average number of neurites per cell body (80 cells in four independent experiments), while the protein expression level of β3-tubulin (**d**) and GAPDH (loading control) were detected from cell lysates by western blot analysis and quantitated by densitometric analysis of the band intensities (normalised to APPL17C treated cultures) (**e**) of four independent experiments. (**f**), quantitating the average number of neurites per cell body (> 80 cells in three independent experiments) following exogenous sAPP695 treatment of either CON, APP_{WT} or APP_{L17C} SH-SY5Y cells. Data represents mean ± SEM. $*p < 0.05$; $**p < 0.01$. Scale bar = 100 μm

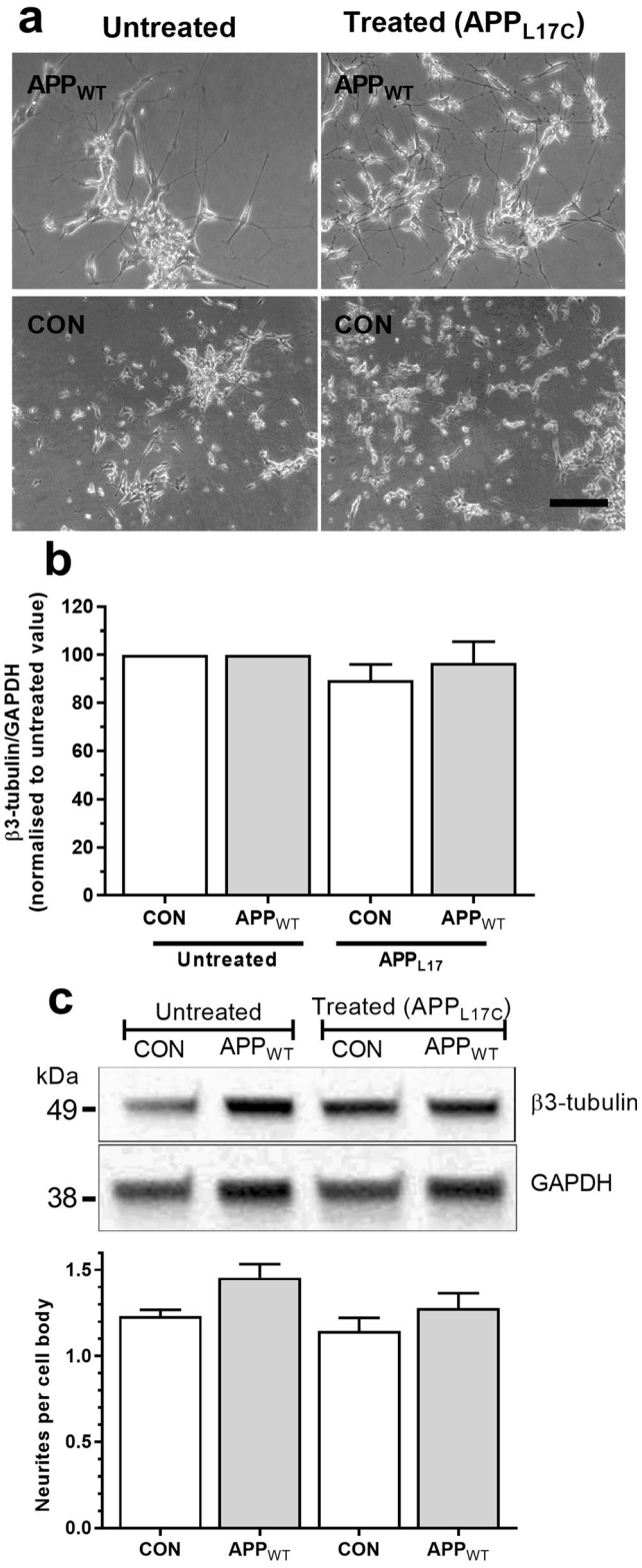

◀ **Fig. 6** The SH-SY5Y APP$_{WT}$ cell line morphology and β3 tubulin expression were unchanged following treatment with conditioned media from APP$_{L17C}$ cultures. **a**–**c** The stably transfected vector control (CON) and APP$_{WT}$ SH-SY5Y cell lines were treated for 3 days using conditioned media taken from APP$_{L17C}$ SH-SY5Y cultures following 14-day differentiation, and the morphological changes were assessed morphologically by viewing phase contrast images (**a**), quantitating the average number of neurites per cell body (80 cells in four independent experiments) (**b**), while the protein expression level of β3-tubulin and GAPDH (loading control) in cell lysates were detected by western blot analysis and densitometric analysis of the band intensities (normalised to untreated cultures) was performed (**c**) from four independent experiments. Data represents mean ± SEM. Scale bar = 100 μm

To determine if the APP$_{L17C}$ cells secreted a neurite outgrowth inhibitory factor, we added 14-day-old differentiated conditioned media from APP$_{L17C}$ cells to the APP$_{WT}$ cells and cultured for a further 3 days and neurite outgrowth monitored morphologically (Fig. 6a). Quantitation of the number of neurites per cell body was unchanged in the APP$_{WT}$ cells treated with conditioned media from APP$_{L17C}$ cultures (Fig. 6b). β3-Tubulin/GAPDH levels showed a similar expression level in the untreated CON and APP$_{WT}$ cells compared to cells treated with APP$_{L17C}$ conditioned media (Fig. 6c). These results indicate that the neurite outgrowth phenotype observed in the APP$_{L17C}$ cells is not due to the secretion of an inhibitory growth factor.

The SH-SY5Y APP$_{L17C}$ Mutant Cell Line Has Increased Rho Activity

RhoA GTPase activity plays an essential role in regulating neurite outgrowth [18, 19]. To test if the RhoA pathway was compromised in the APP$_{L17C}$ cells, we utilised the GLISA RhoA activity assay (small GTPase activation assay). When baseline RhoA activity levels were determined in undifferentiated and differentiated SH-SY5Y cells, we observed a significant increase in RhoA activity in the mutant APP$_{L17C}$ cells compared to the CON and APP$_{WT}$ cells under both conditions (Fig. 7a). Since treating the APP$_{L17C}$ cells with APP$_{WT}$ conditioned media reversed the APP$_{L17C}$ phenotype (Fig. 5d), we examined whether the APP$_{L17C}$ conditioned media treatment modulated RhoA activity. RhoA activity was significantly decreased by approximately 80% in the APP$_{L17C}$ cells treated for 3 days with APP$_{WT}$ conditioned media (Fig. 7b) indicating that the RhoA pathway can be inhibited by factor(s) present in the APP$_{WT}$ conditioned media. We next examined whether inhibiting the RhoA pathway would affect neurite outgrowth in the mutant APP$_{L17C}$ cells by targeting the Rho-associated coiled-coil containing protein kinase (ROCK), the main downstream effector of RhoA kinase activity, with Y-27632 (a highly potent and selective inhibitor ROCK) [18, 20]. Y-27632 treatment (100 μM for 48 h) of the APP$_{L17C}$ cells caused a morphological change to the extent of neurite sprouting (Fig. 7c) with a 4-fold increase in the average number of

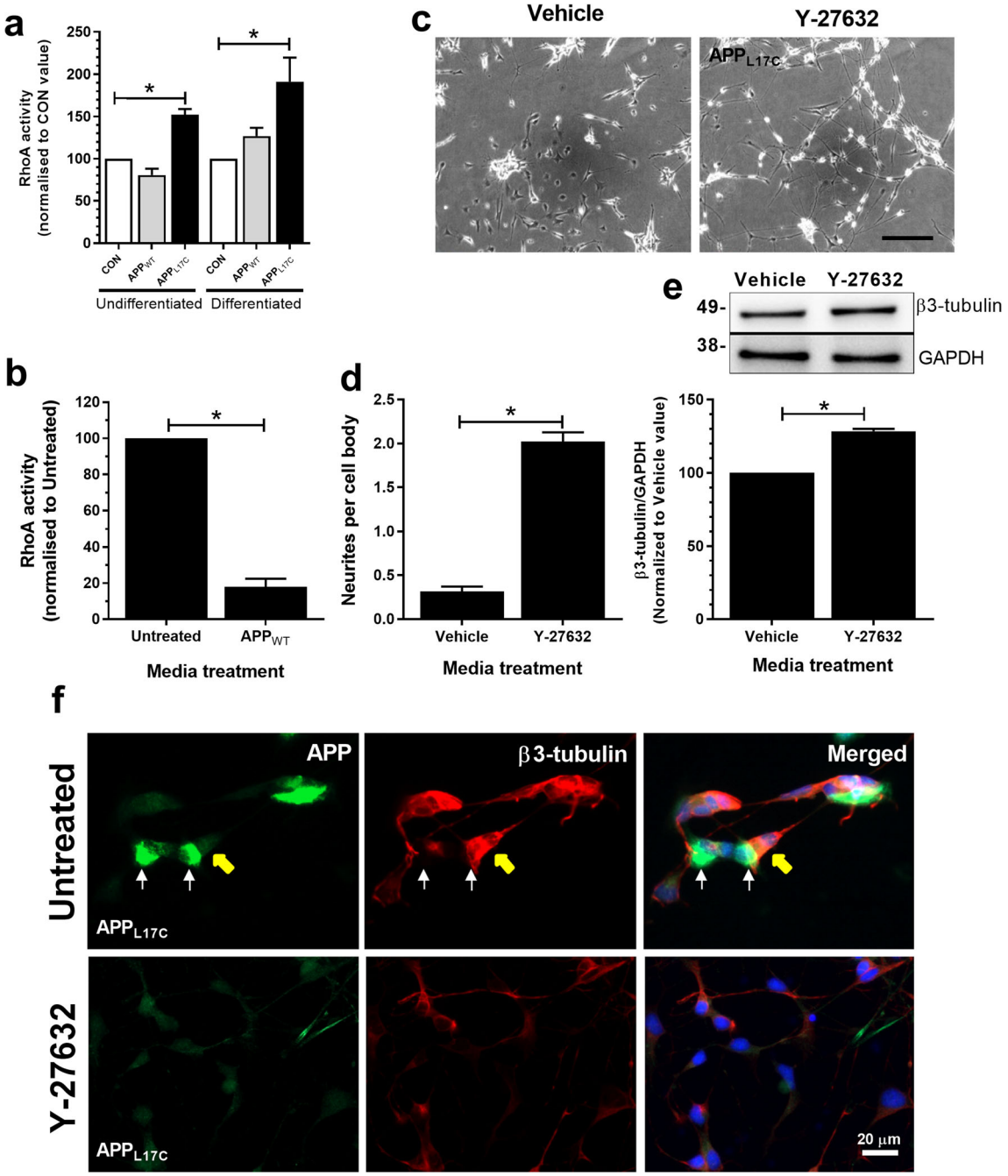

Fig. 7 The SH-SY5Y APP_{L17C} mutant cell line has increased Rho activity. **a**, **b** Rho activity (activated GTP bound to RhoA) was measured in stably transfected vector control (CON), APP_{WT}, APP_{G33I} and APP_{L17C} SH-SY5Y cells under undifferentiated and differentiated (for 14 days in 10 μM retinoic acid) conditions (**a**) and in APP_{L17C}-differentiated cells treated for 3 days with APP_{WT}-conditioned media (**b**). **c**–**f** The SH-SY5Y APP_{L17C}-differentiated cells were treated with a RhoA inhibitor (Y27632), and the morphological changes were assessed morphologically by taking phase contrast images (**c**), quantitating the average number of neurites per cell body (80 cells in four independent experiments) (**d**), measuring the protein expression level of β3-tubulin and GAPDH (loading control) by Western blot analysis and quantitating band intensities by densitometric analysis (data normalised to APP_{L17C}-treated cultures of four independent experiments) €; and by immunofluorescence staining for APP (green) and β3-tubulin (red) and a merged image costained with a DAPI (blue) nuclear marker (**f**). Data represents mean ± SEM. Statistical comparison using ANOVA with $^*p < 0.05$. Scale bars = **c** 100 μm and **f** 20 μm

neurites sprouting per cell body determined, and this was significantly different to the vehicle-treated cells (Fig. 7d). In addition, Y-27632 treatment significantly increased the expression of β3-tubulin/GAPDH levels compared to the control vehicle-treated cells (Fig. 7e) and caused the APP and β3-tubulin immunofluoresence staining pattern (Fig. 7f) to redistribute and display the staining pattern of the APP_{WT} phenotype (Fig. 4a).

Table 1 Top 10 upregulated and downregulated miR genes

		APP_{L17C} vs CON (fold change)		APP_{L17C} vs APP_{wt} (fold change)		APP_{WT} vs CON (fold change)	
Upregulated miRNA genes	Total read	7 days	14 days	7 days	14 days	7 days	14 days
hsa-miR-489-3p	50	5.38**	4.24**	13.09**	7.84**	1.27	− 1.67
hsa-miR-495-3p	56	4.96*	2.20	11.47	4.97**	2.25	− 2.31
hsa-miR-100-5p	2209	2.47	7.39	11.42	4.71	− 2.99	− 2.43
hsa-miR-483-5p	645	1.92	2.08	3.45	3.96	− 1.09	1.15
hsa-miR-483-3p	1117	− 1.28*	− 1.30**	8.53	3.50	1.02	− 2.44
hsa-miR-187-3p	122	3.87	2.37**	8.86	3.20	1.63	− 2.77
hsa-miR-181a-2-3p	2146	2.34	4.05	3.33	3.11	− 1.74	− 1.07
hsa-miR-362-5p	550	2.53	2.35	5.19	2.92	1.08	− 1.78
hsa-miR-501-5p	228	3.33	2.37**	2.88	2.91	1.40	1.01
hsa-miR-181b-5p	4161	5.72	5.01	4.26	2.79	1.14	− 1.53
Downregulated miRNA genes	Total read	7 days	14 days	14 days	7 days	7 days	14 days
hsa-miR-34a-5p	2584	− 120.56	− 101.74	− 50.79	− 96.28	− 1.19	− 1.9
hsa-miR-135b-5p	98	− 11.61*	− 27.62	− 15.82**	− 27.79	2.38**	− 1.76
hsa-miR-124-3p	3264	− 3.38	− 1.81	− 4.49	− 12.07	− 1.87	− 2.69
hsa-miR-33a-5p	259	− 2.12	− 2.12	− 1.82	− 9.39	− 1.00	− 5.16
hsa-miR-1	66	− 7.87	− 2.12	− 1.82	− 8.28**	1.00	− 2.27
hsa-miR-885-5p	90	− 18.69	− 17.27**	− 5.58**	− 7.00	− 1.08	− 1.25
hsa-miR-124-5p	89	− 8.14**	− 10.24	− 3.47	− 5.95	1.26	− 1.72
hsa-miR-137	4968	− 2.18	− 4.11	− 2.42	− 5.52	1.89	− 2.28
hsa-miR-95-3p	1068	− 4.73	− 4.78	− 4.82	− 5.29	1.01	− 1.10
hsa-miR-126-3p	1565	− 2.82	− 3.03	− 4.5	− 4.81	1.08	− 1.07

Upregulated and downregulated miRNA genes expressed in APP_{L17C} compared to CON and APPwt SH-SY5Y cells differentiated in retinoic acid for 7 and 14 days. Student's *t* test comparison: ns, $p > 0.05$; *$p < 0.05$; **$p < 0.01$

miR-34a Expression Is Downregulated in APP_{L17C} Cells, an Effect that Can Be Restored by Treatment with the RhoA Inhibitor

To better understand the molecular basis for the APP_{L17C} neurite outgrowth phenotype, we investigated if it was mediated through changes in microRNA levels. MicroRNAs (miRs) are small noncoding regulatory RNAs that have important roles in neuronal differentiation [21, 22]. We performed next-generation sequencing of miRs from the APP_{L17C}, APP_{WT} and CON cell lines. Sequencing data were analysed using Partek flow for determining the expression levels, significance and reads. We identified over 200 miRs, and the top 10 upregulated and downregulated miR genes, when comparing APP_{L17C} vs. CON, APP_{L17C} vs. APP_{WT} and APP_{WT} vs. CON cell lines, are shown in Table 1. The APP_{WT} cell line analysis was used as the control sample for the mutant APP_{L17C}, and the CON cell line was compared to APP_{WT} to ensure that changes seen in APP_{L17C} were not attributed to APP_{WT} transfection. We performed qRT-PCR on a number of the miRs and found that miR-34a expression was significantly downregulated at 0, 7 and 14 days post-differentiation while miR-124a was significantly lower at 14 days post-differentiation and miR-135b was unchanged (Fig. 8a). Based on these findings, we focused on miR-34a. We tested if miR-34a was linked to RhoA activity in the APP_{L17C} cells by treating 14-day-old differentiated APP_{L17C} cells with the Rho inhibitor, Y-27632. While the miR-34a delta CT ratio was significantly lower in the APPL17C compared to CON cells in Veh-treated cultures (Fig. 8b), treatment of the APPL17C cells with Y-27632 resulted in a significant increase (35-fold higher) in miR-34a expression compared to Veh-treated CON cell levels (Fig. 8c).

Lentiviral Transfection of GFP-miR-34a in APP_{L17C} Cell Line Caused an Increase in Cellular Neurite Outgrowth

Since miR-34a expression was downregulated in mutant APP_{L17C} cells, we examined whether exogenous expression of miR-34a in APP_{L17C} cells would rescue the inhibited neurite outgrowth phenotype. Two experimental paradigms were employed: whether expression of miR-34a prior to the differentiation period would promote neurite outgrowth (i.e., infecting cells 24 h prior to 14 days of differentiation) and secondly

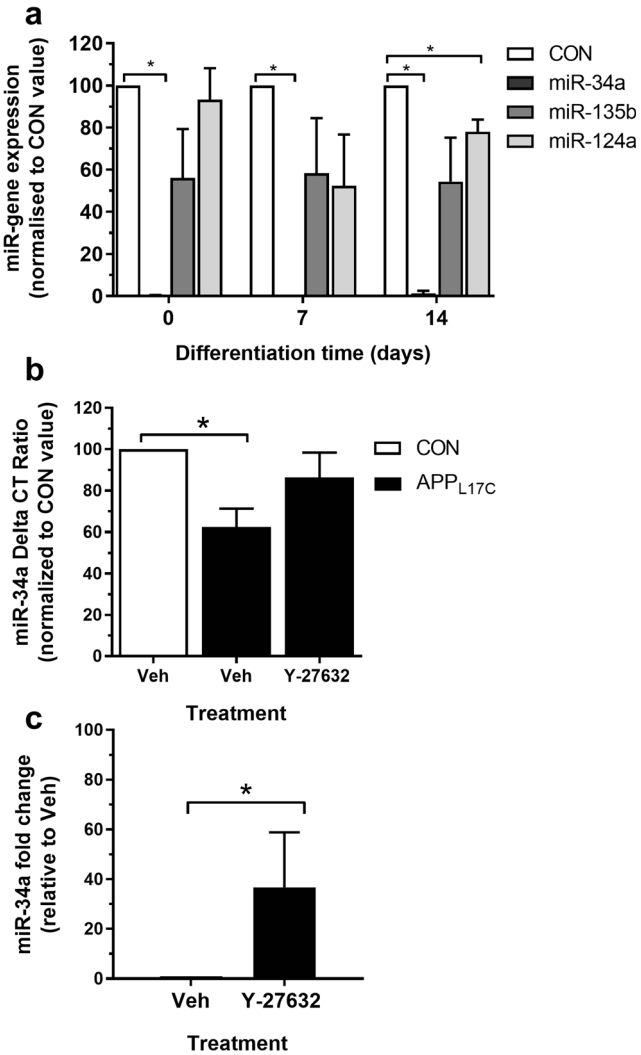

Fig. 8 miR-34a expression is downregulated in APP_{L17C} cells, an effect that can be restored by treatment with the RhoA inhibitor. **a** The stably transfected vector control (CON) and APP_{L17C} SH-SY5Y cell lines were differentiated for 0, 7 and 14 days in 10 μM retinoic acid, and the expression levels of miR-34a (dark grey bar), miR-135b (medium grey bar) and miR-124a (light grey bar) were determined, and the data for each miR was normalised to the concentration calculated for the CON (black bar) cell line. **b** miR-34a delta CT ratio in differentiated APP_{L17C} cells (black bar) treated with 100 μM of the Rho inhibitor, Y27632, for 48 h and normalised to the vehicle (Veh) treated CON cell line (white bar). **c** Fold change of miR-34a expression in APPL17C cells after Y27632 treatment. Data represents mean ± SEM from three to four independent experiments. *$p < 0.05$

whether expression of miR-34a in differentiated cells (i.e., infecting cells post 14 days of differentiation) could rescue the APP_{L17C} phenotype. We transduced miR-34a using the pLenti viral system. The Lenti control (no insert) and Lenti miR-34a constructs (both express GFP) were transduced into the SH-SY5Y APP_{L17C} cell line for 24 h using 20 MOI units of virus. We observed a subset of GPF cells that were positively infected with either the control or miR-34a gene constructs in both the pre- and post-differentiated cell cultures (Fig. 9a). The vector control-infected GFP-positive APP_{L17C} cells showed a lack of neurite outgrowth morphology when infected at either the pre- or post-differentiated periods. In contrast, the GFP-positive miR-34a expressing cells showed a clear morphological change associated with an increase in the number of neurite protrusions from the cell body in both the pre- and post-differentiated cells (Fig. 9a). The number of neurites per cell body in the GFP-positive miR-34a expressing cells was 6-fold higher and significantly different to the CON-infected cells (Fig. 9b). In addition, the neurite lengths in the GFP CON-infected cells were shorter than the diameter of the cell body (~ 6 μm), while in the GFP-positive miR-34a and APP_{L17C} expressing cells, the neurites grew to 20 μm in length, but they remained approximately 2.5-fold shorter and significantly different to the neurite length measured in the differentiated APP_{WT} cells (Fig. 9c).

Discussion

In the central nervous system, APP is mainly expressed in neurons and is best known for its role in the pathogenesis of AD. APP has been associated with roles involving neuroprotection, synaptogenesis, neurite outgrowth, neurodevelopment and metal homeostasis [15, 23–27]. APP exists in a monomer/homodimer equilibrium, and changes to this equilibrium balance alter its post-translational processing, cellular trafficking and localisation [28–30], but the consequences for its physiological function are unclear [31]. It has been shown that Cu-mediated dimerisation can modulate APP-driven synaptogenesis [32]. This study investigated the functional consequences of shifting the APP monomer/homodimer equilibrium balance towards an increased homodimer status in neuronal cells by expressing the mutant APP_{L17C}. The L17C mutation causes a 30% increase in homodimer expression in HEK293 and SH-SY5Y cells [9]. We found that increased expression of APP dimer in the SH-SY5Y cells altered its cellular localisation.

Retinoic acid-induced SH-SY5Y differentiation model is routinely used to promote neuritogenesis by increasing the number and length of neurites from the cell soma [33]. APP is reported to be a major contributing factor for potentiating neuritogenesis as endogenous APP and secreted soluble APP isoforms are elevated in RA-induced SH-SY5Y cell cultures displaying neurite elongation [33]. RA treatment of SH-SY5Y cells increases the expression levels of APP and its homologues, APLP2 and APLP1, at both the mRNA and protein levels, while the secretion of sAPPα in the culture media was elevated [34–36]. Our key finding that the expression of mutant APP_{L17C} in SH-SY5Y cells inhibited neuritogenesis provides further compelling evidence for APP having a regulatory role in neuronal differentiation and morphology. This was supported by the addition of exogenous sAPP695 to the media of APP_{L17C} cells rescuing the neurite growth defect (Fig. 5f), indicating that sAPP could be the neurite outgrowth promoting factor lacking in the APP_{L17C} cells.

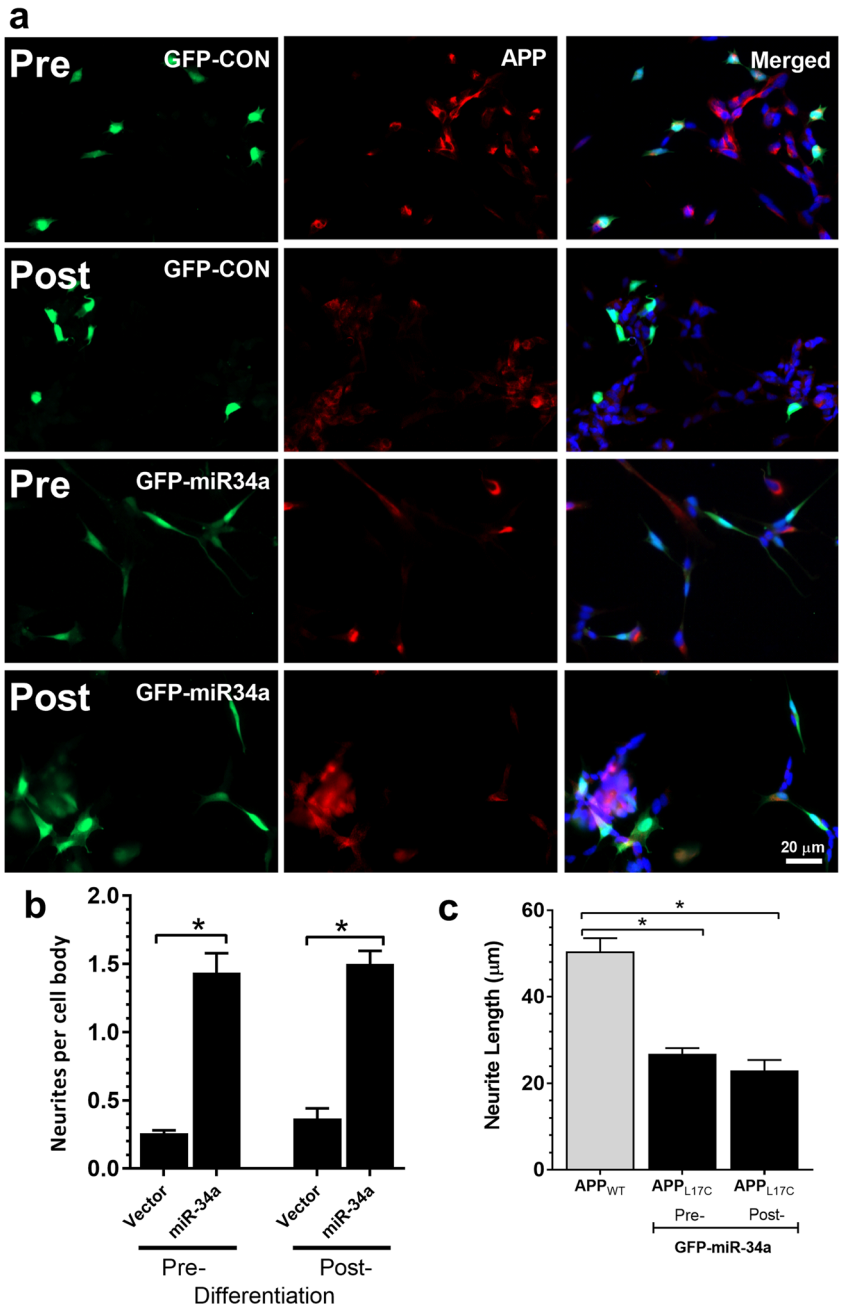

Fig. 9 Lentiviral transfection of GFP-miR-34a in APP_{L17C} cell line caused an increase in cellular neurite outgrowth. **a** APP_{L17C} cells were transduced with either the control empty vector (GFP-CON) or miR-34a vector (GFP-miR-34a) for 24 h either prior to 2 weeks of differentiation (Pre) or following the post-differentiation period (Post) and cultured for a further 3 days before cells were fixed and processed for immunofluorescence histochemistry. Immunofluorescence detection for GFP (green), APP (mAb 22C11, red), and for DAPI nuclear marker (blue) with the channel overlay image (merged) shown. **b**, **c** Analysis from the histological image panels was performed, and the number of neurites/cell body (**b**) was quantified from 40 to 60 cells, and the neurite lengths (**c**) were measured from ~ 90 neurites. Values represent mean ± SEM from three independent experiments. $*p < 0.05$. Scale bar = 100 μM

The intracellular distribution of APP in either RA-treated CON or APP_{WT}-transfected cells revealed a punctate staining pattern for APP immunoreactivity with strong colocalisation with both the cellular markers for ER and Golgi using anti-calnexin and anti-Grasp65 antibodies respectively (Fig. 2). These observations are in agreement with earlier reports describing localisation of APP in both the post-endoplasmic reticulum and Golgi compartments [37, 38]. When mutant APP_{L17C} was transfected into HEK293 cells, it displayed punctate cytoplasmic staining pattern comparable to APP_{WT} and CON-transfected cells [9]. However, when APP_{L17C} was transfected into the SH-SY5Y neuroblastoma cells, a distinct change in the staining pattern for APP was observed; it was restricted to a condensed perinuclear region. This perinuclear immunoreactivity did not colocalise with the Golgi organelle marker, but rather, it strongly colocalised with the ER marker. The overexpression of APP_{L17C} in SH-SY5Y cells not only caused the APP to remain in the ER organelle, but ER trafficking was noticeably affected and found to aggregate or condense to a perinuclear region. It was not surprising that APP_{L17C} was principally located in the ER based on previous reports showing that APP dimerisation is initiated in the ER and formation of the APP dimer causes its retention in this organelle [30, 39]. What is intriguing is that the redistribution

of the ER organelle in these differentiated neuroblastoma cells expressing the mutant APP_{L17C} was not seen in the HEK293-transfected cells [9]. Since ER requires a normal functional microtubule network to move around the cell, we hypothesised that there may be a breakdown of this microtubule network architecture in these mutant transfected cells which would also explain the altered cellular morphology of these cells. This would be consistent with the decreased expression of β3-tubulin levels in the APP_{L17C} cells (Fig. 4).

The Rho family of small GTPases including Rho, Rac and Cdc42 regulates various aspects of the actin cytoskeleton and is a major regulator of neurite outgrowth in the central nervous system [40, 41]. Increased RhoA activity levels are associated with reduced neurite outgrowth [19, 42], and in our APP_{L17C} mutant cells, we found that they exhibited raised levels of RhoA activity in both differentiated and undifferentiated cells compared to the CON-transfected cells. Treating these mutant cells with APP_{WT} conditioned media caused the RhoA activity to decrease 5-fold, and exposing the cells to the Rho inhibitor Y-27632 resulted in increased neuritogenesis and increased β3-tubulin levels (Fig. 7). Taken together, these results indicate that the neurite outgrowth promoting factors may be functioning upstream of RhoA activity in these cells. One possibility is that sAPPα interacts with nerve growth factor (NGF) receptors such as the p75 neurotrophin receptor ($p75^{NTR}$) to promote neurite outgrowth [43] since $p75^{NTR}$ constitutively activates RhoA [44]. It was postulated that downregulation APP reduced the retrograde transport of the NGF receptors, $p75^{NTR}$ and TrkA to the cell surface and that neurons deficient in APP expression, had defects in neurite outgrowth [45]. Other NGF-mediated signalling pathways could also be involved since soluble APP can modulate axonal outgrowth through other pathways such as the MAPK/Erk/Egr1 [46], PI3K/Akt [47] and Akt/GSK-3β/CRMP-2 [48].

A key finding from this study was identifying the neuritogenic activity of APP with the miRNA system. miRNAs are non-coding transcripts of approximately 21 nucleotides that regulate gene expression and have been implicated in various aspects of neuronal development, differentiation, neurogenesis and plasticity as well as in neuronal death and disease; however, the mechanisms underlying the miRNA action are still not well understood (see reviews [49–51]. Using next-generation sequencing, we identified differentially expressed miRs in APP_{L17C} SH-SY5Y cells compared to CON and APP_{WT} cells. We focused our attention on miR-34a, miR-135b and miR-124a which have been associated with stimulating neurite outgrowth and differentiation [52, 53]. Confirmation of the sequencing data with qRT-PCR identified miR-34a as a lead candidate for further investigation since it was downregulated 35-fold in APP_{L17C} cells. miR-34a gene expression is developmentally regulated and has a role in neuronal differentiation and synaptogenesis since manipulation of miR-34a expression altered spinal morphology, neurite outgrowth and synaptic function [54]. The expression level of miR-34a was almost undetectable in APP_{L17C} cells, even in the undifferentiated cell state. miR-34a was affecting the APP_{L17C} phenotype since overexpressing pLenti-miR-34a in the mutant APP_{L17C} cells successfully rescued the morphological phenotype by restoring the number of neurites per cell body to APP_{WT} levels. However, average neurite length remained about 50% the length measured in APP_{WT} cells suggesting that other factors must be contributing to neurite outgrowth in APP_{L17C} cells. We also showed miR-34a expression was linked to RhoA activity since treatment with the RhoA inhibitor Y27632 increased miR-34a levels.

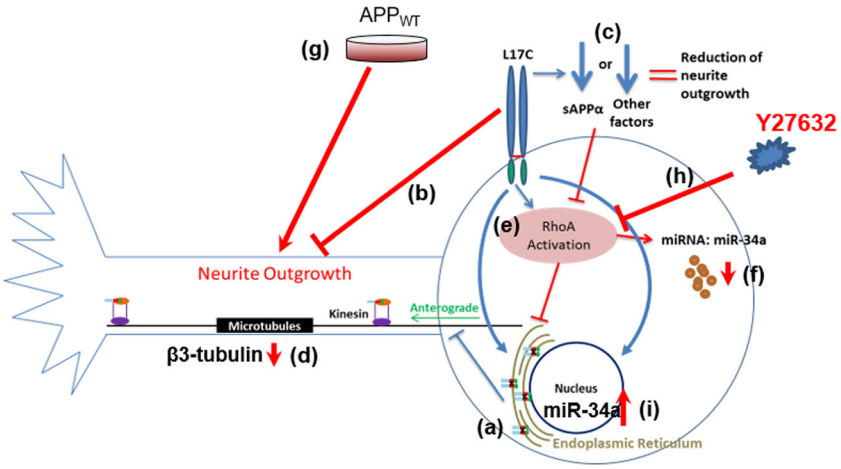

Fig. 10 Schematic representation showing the consequences of increased expression of APP dimersation in the mutant APP_{L17C} SH-SY5Y cell line on modulating neurite outgrowth. Increased APP dimerisation in APP_{L17C} expressing SH-SY5Y neurons caused **a** APP to aggregate in the ER localising to a perinuclear region, **b** inhibition of a neurite outgrowth, **c** failure to secreted neurite outgrowth factors, **d** decreased β3-tubulin expression, **e** increased RhoA activity and **f** decreased miR-34a expression. Rescuing the APP_{L17C} SH-SY5Y neuronal phenotype was achieved by **g** exposing cells to conditioned media from either CON or APP_{WT} cultures and **h** inhibition of RhoA activity using Y27632 (**i**) overexpression of miR-34a gene

We propose that APP regulation of neurite formation acts via miR-34a gene expression, inhibition of Rho activity and modulation of the actin cytoskeleton, and the degree of APP dimerisation directly impacts upon this network (Fig. 10). Taken together, our studies have identified a novel link between APP dimerisation and its physiological function, and linking this to RhoA signalling and miRNA regulation. This has significantly expanded our knowledge of the molecular mechanisms through which the neuritogenic activity of APP is carried out. APP and its family members APLP2 and APLP1 remain an important and interesting group of proteins which deserve more attention given their links to a broad range of physiological processes [2, 3].

Funding Information This work was supported from funding from the Australia National Health and Medical Research Council (R.C., A.F.H.).

Compliance with Ethical Standards

Conflict of Interest The authors declare that they have no conflict of interests.

References

1. Muller UC, Zheng H (2012) Physiological functions of APP family proteins. Cold Spring Harb Perspect Med 2(2):a006288. https://doi.org/10.1101/cshperspect.a006288
2. Muller UC, Deller T, Korte M (2017) Not just amyloid: physiological functions of the amyloid precursor protein family. Nat Rev Neurosci 18(5):281–298. https://doi.org/10.1038/nrn.2017.29
3. Sosa LJ, Caceres A, Dupraz S, Oksdath M, Quiroga S, Lorenzo A (2017) The physiological role of the amyloid precursor protein as an adhesion molecule in the developing nervous system. J Neurochem 143(1):11–29. https://doi.org/10.1111/jnc.14122
4. Thordardottir S, Kinhult Stahlbom A, Almkvist O, Thonberg H, Eriksdotter M, Zetterberg H, Blennow K, Graff C (2017) The effects of different familial Alzheimer's disease mutations on APP processing in vivo. Alzheimers Res Ther 9(1):9. https://doi.org/10.1186/s13195-017-0234-1
5. Gerber H, Wu F, Dimitrov M, Garcia Osuna GM, Fraering PC (2017) Zinc and copper differentially modulate amyloid precursor protein processing by gamma-secretase and amyloid-beta peptide production. J Biol Chem 292(9):3751–3767. https://doi.org/10.1074/jbc.M116.754101
6. Klaver D, Hung AC, Gasperini R, Foa L, Aguilar MI, Small DH (2010) Effect of heparin on APP metabolism and Abeta production in cortical neurons. Neurodegener Dis 7(1–3):187–189. https://doi.org/10.1159/000295661
7. Deyts C, Thinakaran G, Parent AT (2016) APP receptor? To be or not to be. Trends Pharmacol Sci 37(5):390–411. https://doi.org/10.1016/j.tips.2016.01.005
8. Soba P, Eggert S, Wagner K, Zentgraf H, Siehl K, Kreger S, Lower A, Langer A et al (2005) Homo- and heterodimerization of APP family members promotes intercellular adhesion. EMBO J 24(20):3624–3634. https://doi.org/10.1038/sj.emboj.7600824
9. Munter LM, Voigt P, Harmeier A, Kaden D, Gottschalk KE, Weise C, Pipkorn R, Schaefer M et al (2007) GxxxG motifs within the amyloid precursor protein transmembrane sequence are critical for the etiology of Abeta42. EMBO J 26(6):1702–1712. https://doi.org/10.1038/sj.emboj.7601616
10. Kienlen-Campard P, Tasiaux B, Van Hees J, Li M, Huysseune S, Sato T, Fei JZ, Aimoto S et al (2008) Amyloidogenic processing but not amyloid precursor protein (APP) intracellular C-terminal domain production requires a precisely oriented APP dimer assembled by transmembrane GXXXG motifs. J Biol Chem 283(12):7733–7744. https://doi.org/10.1074/jbc.M707142200
11. Qiu WQ, Ferreira A, Miller C, Koo EH, Selkoe DJ (1995) Cell-surface beta-amyloid precursor protein stimulates neurite outgrowth of hippocampal neurons in an isoform-dependent manner. J Neurosci 15(3 Pt 2):2157–2167
12. Alvarez J, Moreno RD, Llanos O, Inestrosa NC, Brandan E, Colby T, Esch FS (1992) Axonal sprouting induced in the sciatic nerve by the amyloid precursor protein (APP) and other antiproteases. Neurosci Lett 144(1–2):130–134. https://doi.org/10.1016/0304-3940(92)90733-N
13. Perez RG, Zheng H, Van der Ploeg LH, Koo EH (1997) The beta-amyloid precursor protein of Alzheimer's disease enhances neuron viability and modulates neuronal polarity. J Neurosci 17(24):9407–9414
14. Williamson TG, Mok SS, Henry A, Cappai R, Lander AD, Nurcombe V, Beyreuther K, Masters CL et al (1996) Secreted glypican binds to the amyloid precursor protein of Alzheimer's disease (APP) and inhibits APP-induced neurite outgrowth. J Biol Chem 271(49):31215–31221. https://doi.org/10.1074/jbc.271.49.31215
15. Allinquant B, Hantraye P, Mailleux P, Moya K, Bouillot C, Prochiantz A (1995) Downregulation of amyloid precursor protein inhibits neurite outgrowth in vitro. J Cell Biol 128(5):919–927. https://doi.org/10.1083/jcb.128.5.919
16. Tuo QZ, Lei P, Jackman KA, Li XL, Xiong H, Li XL, Liuyang ZY, Roisman L et al (2017) Tau-mediated iron export prevents ferroptotic damage after ischemic stroke. Mol Psychiatry 22(11):1520–1530. https://doi.org/10.1038/mp.2017.171
17. Savage C, Hamelin M, Culotti JG, Coulson A, Albertson DG, Chalfie M (1989) Mec-7 is a beta-tubulin gene required for the production of 15-protofilament microtubules in Caenorhabditis elegans. Genes Dev 3(6):870–881. https://doi.org/10.1101/gad.3.6.870
18. Chan CC, Khodarahmi K, Liu J, Sutherland D, Oschipok LW, Steeves JD, Tetzlaff W (2005) Dose-dependent beneficial and detrimental effects of ROCK inhibitor Y27632 on axonal sprouting and functional recovery after rat spinal cord injury. Exp Neurol 196(2):352–364. https://doi.org/10.1016/j.expneurol.2005.08.011
19. Nakayama AY, Harms MB, Luo L (2000) Small GTPases Rac and Rho in the maintenance of dendritic spines and branches in hippocampal pyramidal neurons. J Neurosci 20(14):5329–5338
20. Ishizaki T, Uehata M, Tamechika I, Keel J, Nonomura K, Maekawa M, Narumiya S (2000) Pharmacological properties of Y-27632, a specific inhibitor of rho-associated kinases. Mol Pharmacol 57(5):976–983
21. Makeyev EV, Zhang J, Carrasco MA, Maniatis T (2007) The MicroRNA miR-124 promotes neuronal differentiation by triggering brain-specific alternative pre-mRNA splicing. Mol Cell 27(3):435–448. https://doi.org/10.1016/j.molcel.2007.07.015
22. Schratt GM, Tuebing F, Nigh EA, Kane CG, Sabatini ME, Kiebler M, Greenberg ME (2006) A brain-specific microRNA regulates dendritic spine development. Nature 439(7074):283–289. https://doi.org/10.1038/nature04367
23. Corrigan F, Pham CL, Vink R, Blumbergs PC, Masters CL, van den Heuvel C, Cappai R (2011) The neuroprotective domains of the amyloid precursor protein, in traumatic brain injury, are located in the two growth factor domains. Brain Res 1378:137–143. https://doi.org/10.1016/j.brainres.2010.12.077

24. Dinet V, An N, Ciccotosto GD, Bruban J, Maoui A, Bellingham SA, Hill AF, Andersen OM et al (2011) APP involvement in retinogenesis of mice. Acta Neuropathol 121(3):351–363. https://doi.org/10.1007/s00401-010-0762-2
25. Needham BE, Wlodek ME, Ciccotosto GD, Fam BC, Masters CL, Proietto J, Andrikopoulos S, Cappai R (2008) Identification of the Alzheimer's disease amyloid precursor protein (APP) and its homologue APLP2 as essential modulators of glucose and insulin homeostasis and growth. J Pathol 215(2):155–163. https://doi.org/10.1002/path.2343
26. Needham BE, Ciccotosto GD, Cappai R (2014) Combined deletions of amyloid precursor protein and amyloid precursor-like protein 2 reveal different effects on mouse brain metal homeostasis. Metallomics 6(3):598–603. https://doi.org/10.1039/c3mt00358b
27. Masters CL, Selkoe DJ (2012) Biochemistry of amyloid beta-protein and amyloid deposits in Alzheimer disease. Cold Spring Harb Perspect Med 2(6):a006262. https://doi.org/10.1101/cshperspect.a006262
28. Munter LM, Botev A, Richter L, Hildebrand PW, Althoff V, Weise C, Kaden D, Multhaup G (2010) Aberrant amyloid precursor protein (APP) processing in hereditary forms of Alzheimer disease caused by APP familial Alzheimer disease mutations can be rescued by mutations in the APP GxxxG motif. J Biol Chem 285(28):21636–21643. https://doi.org/10.1074/jbc.M109.088005
29. Noda Y, Asada M, Kubota M, Maesako M, Watanabe K, Uemura M, Kihara T, Shimohama S et al (2013) Copper enhances APP dimerization and promotes Abeta production. Neurosci Lett 547:10–15. https://doi.org/10.1016/j.neulet.2013.04.057
30. Isbert S, Wagner K, Eggert S, Schweitzer A, Multhaup G, Weggen S, Kins S, Pietrzik CU (2012) APP dimer formation is initiated in the endoplasmic reticulum and differs between APP isoforms. Cell Mol Life Sci 69(8):1353–1375. https://doi.org/10.1007/s00018-011-0882-4
31. Khalifa NB, Van Hees J, Tasiaux B, Huysseune S, Smith SO, Constantinescu SN, Octave JN, Kienlen-Campard P (2010) What is the role of amyloid precursor protein dimerization? Cell Adhes Migr 4(2):268–272
32. Baumkotter F, Schmidt N, Vargas C, Schilling S, Weber R, Wagner K, Fiedler S, Klug W et al (2014) Amyloid precursor protein dimerization and synaptogenic function depend on copper binding to the growth factor-like domain. J Neurosci 34(33):11159–11172. https://doi.org/10.1523/jneurosci.0180-14.2014
33. da Rocha JF, da Cruz e Silva OA, Vieira SI (2015) Analysis of the amyloid precursor protein role in neuritogenesis reveals a biphasic SH-SY5Y neuronal cell differentiation model. J Neurochem 134(2):288–301. https://doi.org/10.1111/jnc.13133
34. Adlerz L, Beckman M, Holback S, Tehranian R, Cortes Toro V, Iverfeldt K (2003) Accumulation of the amyloid precursor-like protein APLP2 and reduction of APLP1 in retinoic acid-differentiated human neuroblastoma cells upon curcumin-induced neurite retraction. Brain Res Mol Brain Res 119(1):62–72. https://doi.org/10.1016/j.molbrainres.2003.08.014
35. Holback S, Adlerz L, Iverfeldt K (2005) Increased processing of APLP2 and APP with concomitant formation of APP intracellular domains in BDNF and retinoic acid-differentiated human neuroblastoma cells. J Neurochem 95(4):1059–1068. https://doi.org/10.1111/j.1471-4159.2005.03440.x
36. Vella LJ, Cappai R (2012) Identification of a novel amyloid precursor protein processing pathway that generates secreted N-terminal fragments. FASEB J 26(7):2930–2940. https://doi.org/10.1096/fj.11-200295
37. LeBlanc AC, Goodyer CG (1999) Role of endoplasmic reticulum, endosomal-lysosomal compartments, and microtubules in amyloid precursor protein metabolism of human neurons. J Neurochem 72(5):1832–1842. https://doi.org/10.1046/j.1471-4159.1999.0721832.x
38. Greenfield JP, Tsai J, Gouras GK, Hai B, Thinakaran G, Checler F, Sisodia SS, Greengard P et al (1999) Endoplasmic reticulum and trans-Golgi network generate distinct populations of Alzheimer β-amyloid peptides. Proc Natl Acad Sci U S A 96(2):742–747. https://doi.org/10.1073/pnas.96.2.742
39. Ben Khalifa N, Tyteca D, Marinangeli C, Depuydt M, Collet JF, Courtoy PJ, Renauld JC, Constantinescu S et al (2012) Structural features of the KPI domain control APP dimerization, trafficking, and processing. FASEB J 26(2):855–867. https://doi.org/10.1096/fj.11-190207
40. Chen C, Wirth A, Ponimaskin E (2012) Cdc42: an important regulator of neuronal morphology. Int J Biochem Cell Biol 44(3):447–451. https://doi.org/10.1016/j.biocel.2011.11.022
41. Fujita Y, Yamashita T (2014) Axon growth inhibition by RhoA/ROCK in the central nervous system. Front Neurosci 8:338. https://doi.org/10.3389/fnins.2014.00338
42. Kranenburg O, Poland M, Gebbink M, Oomen L, Moolenaar WH (1997) Dissociation of LPA-induced cytoskeletal contraction from stress fiber formation by differential localization of RhoA. J Cell Sci 110 (Pt 19) (19):2417–2427
43. Hasebe N, Fujita Y, Ueno M, Yoshimura K, Fujino Y, Yamashita T (2013) Soluble beta-amyloid precursor protein alpha binds to p75 neurotrophin receptor to promote neurite outgrowth. PLoS One 8(12):e82321. https://doi.org/10.1371/journal.pone.0082321
44. Yamashita T, Tucker KL, Barde YA (1999) Neurotrophin binding to the p75 receptor modulates Rho activity and axonal outgrowth. Neuron 24(3):585–593. https://doi.org/10.1016/S0896-6273(00)81114-9
45. Zhang YW, Chen Y, Liu Y, Zhao Y, Liao FF, Xu H (2013) APP regulates NGF receptor trafficking and NGF-mediated neuronal differentiation and survival. PLoS One 8(11):e80571. https://doi.org/10.1371/journal.pone.0080571
46. Chasseigneaux S, Dinc L, Rose C, Chabret C, Coulpier F, Topilko P, Mauger G, Allinquant B (2011) Secreted amyloid precursor protein beta and secreted amyloid precursor protein alpha induce axon outgrowth in vitro through Egr1 signaling pathway. PLoS One 6(1):e16301. https://doi.org/10.1371/journal.pone.0016301
47. Gu X, Meng S, Liu S, Jia C, Fang Y, Li S, Fu C, Song Q et al (2014) miR-124 represses ROCK1 expression to promote neurite elongation through activation of the PI3K/Akt signal pathway. J Mol Neurosci 52(1):156–165. https://doi.org/10.1007/s12031-013-0190-6
48. Fang W, Gao G, Zhao H, Xia Y, Guo X, Li N, Li Y, Yang Y et al (2015) Role of the Akt/GSK-3beta/CRMP-2 pathway in axon degeneration of dopaminergic neurons resulting from MPP+ toxicity. Brain Res 1602:9–19. https://doi.org/10.1016/j.brainres.2014.08.030
49. Carrel D, Firestein BL (2009) MicroRNA-mediated regulation of synaptic palmitoylation: shrinking fat spines. Nat Cell Biol 11(6):681–682. https://doi.org/10.1038/ncb0609-681
50. Schratt G (2009) microRNAs at the synapse. Nat Rev Neurosci 10(12):842–849. https://doi.org/10.1038/nrn2763
51. Nampoothiri SS, Rajanikant GK (2017) Decoding the ubiquitous role of microRNAs in neurogenesis. Mol Neurobiol 54(3):2003–2011. https://doi.org/10.1007/s12035-016-9797-2
52. Jang J, Lee S, Oh HJ, Choi Y, Choi JH, Hwang DW, Lee DS (2016) Fluorescence imaging of in vivo miR-124a-induced neurogenesis of neuronal progenitor cells using neuron-specific reporters. EJNMMI Res 6(1):38. https://doi.org/10.1186/s13550-016-0190-y
53. Lin L, Gu X, Liu S, Wang X (2014) miR-124a promotes neurite outgrowth by inhibiting iASPP expression. Nan Fang Yi Ke Da Xue Xue Bao 34(1):31–35. https://doi.org/10.3969/j.issn.1673-4254.2014.01.07
54. Agostini M, Tucci P, Steinert JR, Shalom-Feuerstein R, Rouleau M, Aberdam D, Forsythe ID, Young KW et al (2011) microRNA-34a regulates neurite outgrowth, spinal morphology, and function. Proc Natl Acad Sci U S A 108(52):21099–21104. https://doi.org/10.1073/pnas.1112063108